Tuning the optical properties of planar photonic crystals by liquid crystal infiltration

J. Martz[a], B. Wild[b], R. Ferrini[*a], L.A. Dunbar[b], M. Mulot[**c], S. Anand[c], R. Houdré[b], L. Zuppiroli[a]

[a]Laboratoire d'Optoélectronique des Matériaux Moléculaires,
École Polytechnique Fédérale de Lausanne (EPFL), CH-1015 Lausanne, Switzerland
[b]Institut de Photonique et d'Electronique Quantique,
École Polytechnique Fédérale de Lausanne (EPFL), CH-1015 Lausanne, Switzerland
[c]Department of Microelectronics and Information Technology,
Royal Institute of Technology (KTH), S-16440 Kista, Sweden

ABSTRACT

Recently there has been a growing amount of attention devoted to tuneable photonic crystals (PhCs) where the optical response of PhC structures can be dynamically modified. We will show how infiltrating planar PhCs with a synthetic organic material allows the trimming and tuning of their optical properties. The potential of PhC infiltration will be demonstrated for InP-based planar PhCs consisting of a hexagonal array of air holes (hole diameter = 200 – 400 nm; air filling factor = 0.40-0.50) etched through a planar waveguide in which light emitters (*i.e.* quantum wells) were embedded to enable optical measurements. The PhC pores were infiltrated with LC-K15 (5CB) nematic liquid crystals (LCs) in a specifically designed vacuum chamber, thereby changing the refractive index contrast between the holes and the semiconductor (*trimming*). Moreover, the possibility of *tuning* the optical response of PhCs by an external perturbation (*i.e.* temperature) was demonstrated. The change of the PhC optical properties due to infiltration and temperature tuning was studied both experimentally and theoretically. Experimental measurements were compared to theoretical calculations in order to obtain information on the in-filling efficiency, the LC refractive index, and the molecule orientation inside the holes. In the first case, optical measurements were performed as a function of temperature, whilst the average LC director configuration was determined by comparing transmission spectra in the transverse electric and magnetic polarization directions.

Keywords: photonic crystals, optical properties, tuneable photonic bandgap materials, liquid crystals.

1. INTRODUCTION

In recent years great effort has been devoted to the study of photonic crystals (PhCs), which are a new class of artificial materials that offer the possibility to control light propagation at a wavelength scale.[1] They consist of a periodic arrangement of dielectric or metallic elements in one, two or three dimensions. The periodicity of these dielectric structures affects the properties of photons in the same way as the periodic potential affects the properties of electrons in semiconductor crystals. Thus, light propagation along particular directions is forbidden within large energy bands known as photonic bandgaps. Using these properties, novel applications and devices have been proposed and experimentally demonstrated in different fields from quantum optics to integrated optics:[1] PhC-based optical cavities with high quality factors have been proposed for the demonstration of cavity quantum electro-dynamic effects such as the control of spontaneous emission or the fabrication of single photon sources. Moreover, PhC devices have been proposed as building blocks in wavelength division multiplexing applications for integrated optics. Unfortunately, there are still many factors limiting their use in real devices, such as fabrication imperfections, losses and temperature sensitivity. Infiltrating the pores of a PhC with a synthetic organic material that has a tuneable refractive index can overcome some of these factors by either controlling the optical properties of the PhC on demand (*tuning*) or compensating fabrication imperfections of the PhC itself (*trimming*).

---

*rolando.ferrini@epfl.ch; phone +41 (0)21 693 34 46; fax +41 (0)21 693 44 70; lomm.epfl.ch
**Present address*: Optoelectronics Laboratory, Helsinki University of Technology, FL-02015 TKK Helsinki, Finland.

The optical properties of PhCs can be tuned by modifying the optical length of the PhC structure. This can be achieved either by adjusting the geometrical parameters that define the PhC lattice (*e.g.* the lattice period) or by changing the refractive indexes of the PhC components. In the first case a mechanical stress may be applied to the PhC slab,[2] whilst in the second approach it is possible to act either on the high index or on the low index component. In particular, the refractive index of the high index (*e.g.* the semiconductor) medium can be modified by applying an external magnetic or electric field.[3-4] Equally, the low index element (*e.g.* the air) can be replaced by a different material which offer further degrees of tuneability. For example, the potential of PhC infiltration with liquid crystals (LCs) have been already demonstrated for one-, two- and three-dimensional (1D, 2D and 3D) PhCs.[1,5-22] Due to the molecule shape and alignment, LCs exhibit an optical anisotropy (birefringence) and an ordered LC structure can be easily and reversibly modulated by means of external perturbations, thus providing a change of the refractive index on demand. The tuning of the optical properties of several PhC structures has been demonstrated using either the temperature,[10,13-16,18] or an electrical field[12,19-21] or a photonic source[17,22] as external perturbations.

Preliminary studies demonstrated the possibility of tuning the optical properties of GaAs-based planar PhC structures by infiltration with nematic LCs.[13] This emerging research topic may have a huge technological impact in various application fields. For instance, a PhC microcavity with a quality factor $Q \approx n/\Delta n$ can be used to measure a variation Δn of the refractive index of the in-filled material, whilst the selection of single optical channels with a 100 GHz spacing translates into $\Delta n/n \approx 5 \times 10^{-4}$. In this communication we will show how infiltrating InP-based planar PhC devices with LCs allows one to change the refractive index contrast between the holes and the semiconductor (*trimming*) and to *tune* the optical response of the PhCs by an external perturbation (*i.e.* temperature). InP-based planar PhCs consisting of a hexagonal array of air holes (hole diameter = 200 – 400 nm; air filling factor = 0.40-0.50) were infiltrated with LC-K15 (5CB) nematic LCs in a vacuum chamber specifically designed to empty the gaseous content of the holes, to clean and, when necessary, to chemically activate the device surface.[23] Optical measurements were compared to theoretical calculations in order to obtain information on the in-filling efficiency, the LC refractive index and the orientation of the molecules inside the holes. In the first case, optical measurements were performed as a function of temperature, whilst the average LC director configuration was determined by comparing transmission spectra in different polarization directions.

2. SAMPLE DESCRIPTION AND CHARACTERIZATION

Planar PhCs consisting of a triangular lattice of air holes were etched through a nominally undoped InP/(Ga,In)(As,P)/InP vertical waveguide grown by metalorganic vapor phase epitaxy on a (100) *n*-doped InP substrate [see Fig. 1(a)].[24]
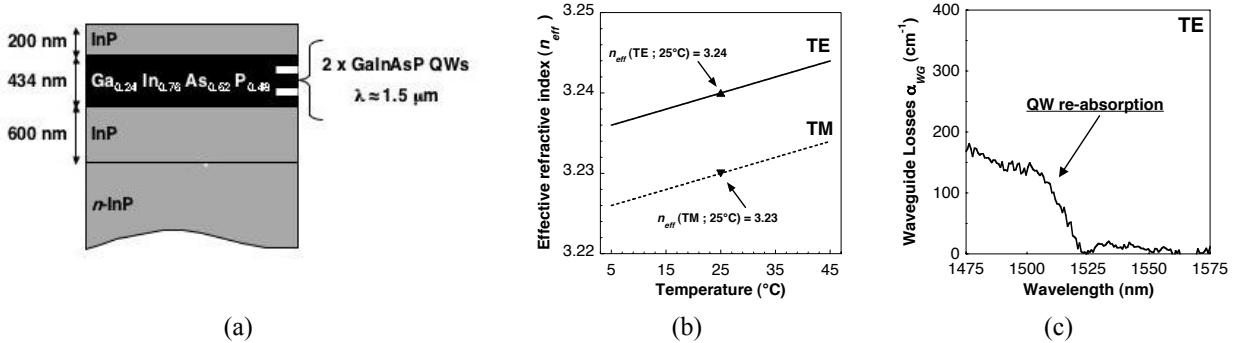
Figure 1: (a) InP/GaInAsP/InP planar waveguide. Two GaInAsP quantum wells (QWs) are embedded in the $Ga_{0.24}In_{0.78}As_{0.52}P_{0.48}$ core layer: the photoluminescence spectrum is centered at $\lambda = 1.5$ μm;[24] (b) effective refractive index n_{eff} of both the TE and TM guided modes as a function of temperature;[25] (c) modal losses α_{WG} measured along the waveguide for the TE mode.[26]

The GaInAsP layer was lattice matched to InP with a direct bandgap emission wavelength $\lambda = 1.22$ μm. The InP top cladding and the GaInAsP core are 200 and 434 nm thick, respectively. In the spectral region of interest (*i.e.* $\lambda \sim 1.55$ μm) the refractive index values of the core and the cladding layers are n(GaInAsP) = 3.35 and n(InP) = 3.17,

respectively, and the waveguide is monomode in both the transverse electric (TE) and magnetic (TM) polarization directions. The effective refractive index n_{eff} values of both the TE and TM guided modes are reported in Fig. 1(b) as a function of temperature.[25] An internal light source (ILS) was embedded in the core layer for optical measurements:[24] it consists of two different GaInAsP strain-compensated quantum wells (QWs) emitting at 1.47 and 1.55 µm, respectively. They are separated by a 30 nm spacer and located approximately in the middle of the guiding structure between two 181 nm-thick barrier layers. The superimposition of the two QW emission peaks yields a 100 nm-wide photoluminescence (PL) spectrum centered at $\lambda = 1.5$ µm.[24] Part of the PL signal propagates parallel to the surface as a guided mode but, due to the presence of the QWs inside the core, it is strongly affected by the QW reabsorption. The modal losses α_{WG} measured along the waveguide for the TE mode are shown in Fig. 1(c).[26]

The PhC structures were fabricated by electron beam lithography and chemically assisted ion beam etching (CAIBE).[26] A scanning electron microscopy cut view of the obtained PhCs appears in Fig. 2(a): the hole depth d is of the order of 4 µm. Due to the limited spectral width of the ILS the "lithographic tuning" approach was adopted and the same PhC structures were repeated for different values of the lattice period a (*i.e.* $a = 280$-580 nm with $\Delta a = 20$ nm). When the air filling factor f is kept constant (its intended value was $f = 0.40$-0.50, corresponding to an hole diameter $D = 200 - 400$ nm), the scaling property of PhCs[1] allows one to scan the whole photonic bandgap as a function of the normalized energy $u = a/\lambda$ (reduced units). Two types of structures were fabricated: (*i*) 8-rows thick ΓM-oriented PhC slabs [see Fig. 2(b)] and (*ii*) Fabry-Pérot (FP) cavities between two 4-rows thick ΓM-oriented PhC mirrors separated by a spacer W [see Fig. 2(c)].

(a)   (b)   (c)
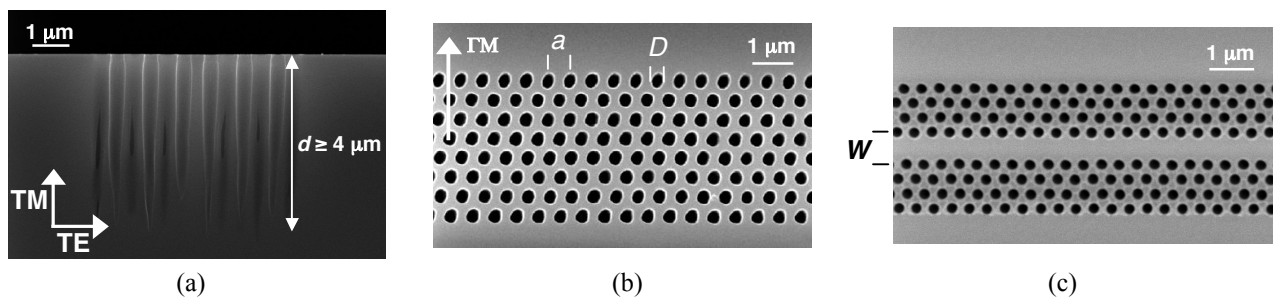
Figure 2: *Scanning electron microscopy* - (a) Cut view of a PhC: the hole depth is $d \geq 4$ µm. The white arrows indicate the orientation of the electric field for the transverse electric (TE) and magnetic (TM) polarization directions. Top view of (b) a 8-rows thick ΓM-oriented PhC slab (*a*: lattice period; *D*: hole diameter) and (c) a Fabry-Pérot cavity between two 4-rows thick ΓM-oriented PhC mirrors (*W*: cavity width).

An ILS technique[24] was used to optically characterize the infiltrated PhC structures. The PL excited inside the QWs is used as a built-in probe beam. Part of the PL signal propagates parallel to the surface as a guided mode and interacts with the PC structure before escaping from a cleaved edge where adequate light collection is performed. The absolute transmission through the PhC structure was obtained by normalizing the spectrum measured after transmission through the PhC with respect to a spectrum collected in a non-patterned region of the sample. Details on both the experimental set-up and the technique are given in Ref. (24). Measurements as a function of temperature were performed by mounting the sample on a Peltier stage which allows one to tune the temperature of the sample in the range $\Delta T = 60$ °C:[25] The temperature was varied from T = 25 °C up to T = 40 °C and a silver paste was used to mount the sample on the Peltier stage and to provide good thermal contact.

The TE transmission spectra at room temperature (T = 25 °C) through 8-rows thick ΓM-oriented slabs are shown in Fig. 3(a) (black lines). A well-defined stopgap with steep band edges appears in the frequency range $u = 0.22 - 0.33$. Transmission values as high as 60% and 30% are reached for $u < 0.2$ (dielectric band) and $u > 0.33$ (air band), respectively. The spectrum was fitted by means of a two-dimensional finite difference time domain (2D-FDTD) model assuming the vertical waveguide effective refractive index as the matrix index [$n_{eff} = 3.24$ for the TE guided mode at room temperature:[25] see Fig. 1(b)] and $n_{hole} = 1$ as the hole refractive index.[27] Out-of-plane losses were included into the 2D model by adding a phenomenological imaginary dielectric constant ε'' in the air holes.[28] The fit parameters were the air-filling factor f and ε''. The calculated spectrum is shown in Fig. 3(a) (light grey dotted lines). Higher f and ε'' values

are found at the dielectric band edge (*i.e.* $f = 0.50 \pm 0.01$ and $\varepsilon'' = 0.104 \pm 0.001$) than at the air band edge (*i.e.* $f = 0.42 \pm 0.01$ and $\varepsilon'' = 0.045 \pm 0.001$), thus indicating a widening of the holes with respect to their intended diameter due to chemical etching.[26] Moreover, while the obtained loss values indicate that, as for most of the present PhC-etching techniques, the holes are cylindro-conical with a cone angle value $\leq 1°$,[26,28] the increase of ε'' with the photon energy doesn't follow the usual scaling law $\varepsilon'' \propto (u^2 \times f)$.[28] This discrepancy can be attributed to the feature size dependent etching ("lag effect") of InP-based PhCs.[26]
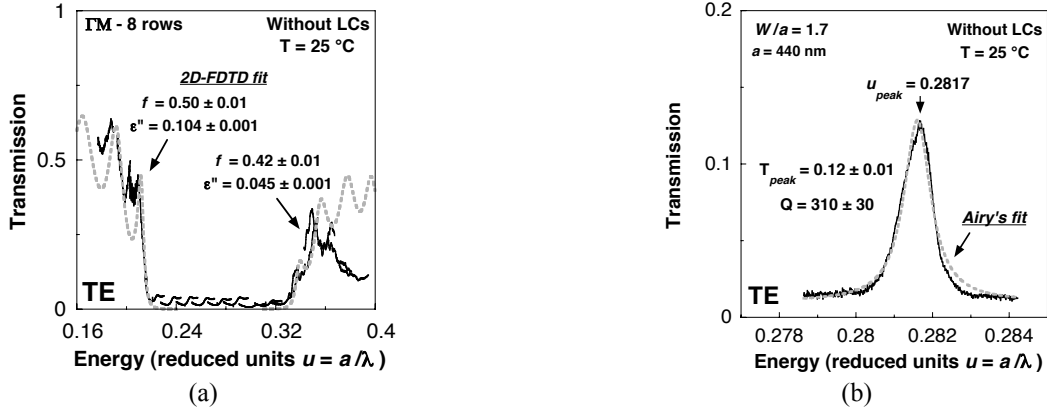
Figure 3: *Without liquid crystals (T = 25 °C)* - Experimental (black lines) and calculated (light grey dotted lines) TE transmission spectra through (a) 8-rows thick ΓM-oriented PhC slabs and (b) a Fabry-Pérot (FP) cavity between two 4-rows thick ΓM-oriented PhC mirrors [see Figs. 2(b) and (c)]. (a) The values of the air filling factor *f* and the loss parameter ε'' obtained from the 2D-FDTD fit of the dielectric and the air transmission bands are reported, respectively. (b) The resonance energy u_{peak}, the peak transmission T_{peak} and the cavity quality factor Q are indicated. The result of the Airy's fit of the FP resonance [see Eq. (1)] is summarized in Table 1.

A transmission spectrum at room temperature through a FP cavity is shown in Fig. 3(b). For $W/a = 1.7$ and $a = 440$ nm a FP resonance is found at the energy $u_{peak} = 0.2817$ (*i.e.* $\lambda_{peak} = a/u_{peak} = 1562$ nm), with a peak transmission $T_{peak} = 0.12 \pm 0.01$ and a cavity quality factor $Q = 310 \pm 30$.[26] The resonance energy u_{peak} was fitted both by a 2D-FDTD model and by a 2D plane wave expansion (PWE) method[29] assuming $n_{eff} = 3.24$ as the matrix index,[25] $n_{hole} = 1$ as the hole refractive index (see above), and *f* as a free fitting parameter: the value $f = 0.47 \pm 0.02$ was obtained. The FP peak was fitted using the Airy's formula[24]

$$ T_{FP} = T_{base} + \frac{T_{4\,rows}^2}{\left| 1 - R_{4\,rows}\, e^{2\,i\,\varphi}\, e^{-\alpha_{WG} W} \right|^2} \tag{1} $$

where the free fitting parameters are $T_{4\,rows}$ and $R_{4\,rows}$, *i.e.* the transmission and the reflection coefficients for a single 4-rows thick PhC mirror, respectively. φ is the normal incidence round-trip phase. T_{base} is the excess transmission inside the bandgap typical of InP-based PhCs:[24] here $T_{base} = 0.01$ and is assumed to be independent from the n_{hole} value. The factor $\exp(-\alpha_{WG} W)$ takes into account the modal absorption α_{WG} inside the cavity: since the FP peak is located in the wavelength region where the QW reabsorption is negligible $\alpha_{WG} = 0$ [see Fig. 1(c)].[26] The calculated Airy's curve is shown in Fig. 3(b) (light grey dotted line) and the result of the fit is summarized in Table 1.

	Temperature	$T_{4\,rows}$	$R_{4\,rows}$	$L_{4\,rows} = 1 - T_{base} - T_{4\,rows} - R_{4\,rows}$
Without LCs	25 °C	0.013 ± 0.005	0.960 ± 0.005	0.017
With LCs	25 °C	0.090 ± 0.005	0.887 ± 0.005	0.013
	40 °C	0.090 ± 0.005	0.865 ± 0.005	0.035

Table 1: Transmission ($T_{4\,rows}$), reflection ($R_{4\,rows}$) and loss ($L_{4\,rows}$) coefficients of a single PhC mirror *without* (T = 25 °C) and *with* (T = 25 and 40 °C) liquid crystals as obtained from the Airy's fit of the transmission resonance of a Fabry-Pérot cavity between two 4-rows thick ΓM-oriented slabs separated by a spacer $W/a = 1.7$ [see Figs. 2(b) and (c)].

3. LIQUID CRYSTAL INFILTRATION

3.1 Nematic liquid crystals [*i.e.* LC-K15 (5CB)]

The fabricated InP-based PhCs were infiltrated with nematic LCs. In Ref. (13) preliminary infiltration experiments were performed on GaAs-based PhCs with LC-E7 from Merck, a blend of cyanoterphenyl and several cyanobiphenyl molecules. Here, LC-K15 from Merck was used: while maintaining the same wettability as LC-E7 on the semiconductor surface,[23] LC-K15 consists of only one type of molecules [4-cyano-4'-pentylbiphenyl (5CB) : see the inset of Fig. 4(a)]. The latter property guarantees the stability of LC-K15 with respect to the infiltration procedure (see Sect. 3.3). This was checked by means of differential scanning calorimetry measurements.[30] The response of the LC-K15 was analysed *before* and *after* [grey and black lines in Fig. 4(a), respectively] heating the LC bulk material up to 110 °C at a pressure of 10^{-6} mbar (*i.e.* the same conditions as during the in-filling process: see Sect. 3.3). The peaks in the heat capacity signals reported in Fig. 4(a) and corresponding to the nematic-to-isotropic phase transition[30] are located at the same temperature, thus showing that the composition as well as the optical properties (*i.e.* the refractive index) of LC-K15 do not undergo to any modification after the infiltration process. We remark that LC-K15 presents another advantage with respect to LC-E7: the lower nematic-to-isotropic and nematic-to-polycrystalline phase transition temperatures $T_{c1} = 35.1$ °C (clearing point) [see also Fig. 4(a)] and $T_{c2} = 23$ °C (melting point), respectively. This makes LC-K15 more suitable than LC-E7 for temperature tuning experiments (see Sect. 4.3). The ordinary n_o, extraordinary n_e, and isotropic n_i refractive index values of LC-K15 as a function of temperature are reported in Fig. 4(b): the data were derived from Ref. (31) for a wavelength $\lambda = 1.5$ μm.

(a)   (b)
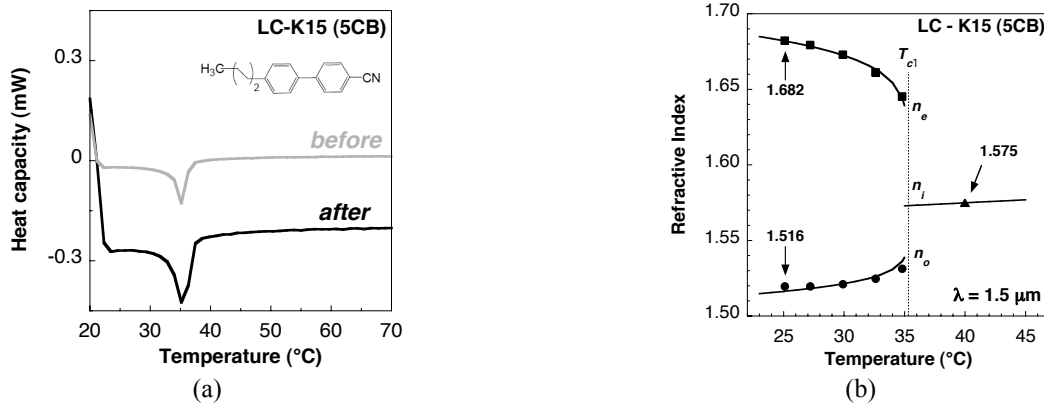
Figure 4: *Liquid crystals LC-K15 (5CB)* – (a) Differential scanning calorimetry spectrum of LC-K15 *before* (grey line) and *after* (black line) heating up to 110 °C at a pressure of 10^{-6} mbar. The chemical composition of LC-K15 is reported in the inset. (b) Ordinary n_o, extraordinary n_e, and isotropic n_i refractive index values of LC-K15 as a function of temperature: the data were derived from Ref. (31) for a wavelength $\lambda = 1.5$ μm. The nematic-to-isotropic phase transition temperature [T_{c1} (clearing point)] is indicated.

3.2 Infiltration technology

The physical infiltration of porous materials with LCs is a relatively simple procedure that is assisted by the capillary forces. In the case of 3D or membrane-based planar PhCs the samples can be partially immersed in a LC bath and, while the capillary forces help the LC molecules to penetrate into the pores, the air is naturally evacuated. On the other hand, in substrate-based planar PhCs the air holes are accessible only from the top and the elimination of air (and any other molecule) from the pores is more difficult. It has been indeed demonstrated[13-14] that working under vacuum can help the infiltration process and minimize the effects of gas trapping either in the sample or in the LC blend. To this extent a specifically designed vacuum chamber was built for infiltration experiments (see Fig. 5). The chamber is equipped to enable PhC surface cleaning by low-power plasma, control of temperature and gas flows during the infiltration procedure, and, when necessary, chemical surface modification by molecule grafting.[23]
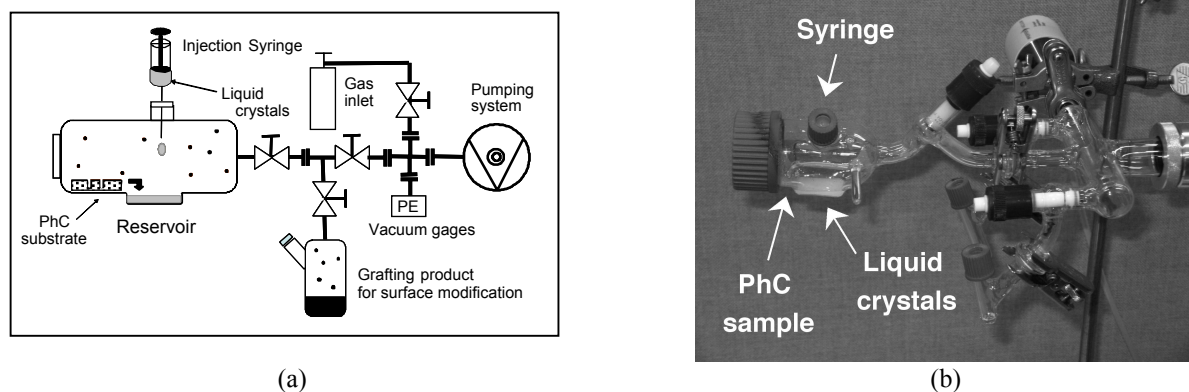
Figure 5: *Infiltration* – (a) High vacuum system for PhC infiltration experiments. (b) Infiltration chamber.

3.3 Infiltration procedure

As for the in-filling procedure, the best conditions for temperature, pressure and infiltration time were investigated to optimize the process and increase its reproducibility. The entire procedure can be divided into three steps: (*i*) *Evacuation*: The vacuum chamber is pumped and heated, thus emptying the gaseous content of the holes and degassing the LC blend. (*ii*) *Contact*: Once a steady state is reached with a base pressure of 10^{-6} mbar, the PhC sample is ready to be filled and is brought in contact with the LCs either by deposing a LC drop on the photonic crystal surface with a syringe or by immersing the sample into the reservoir. (*iii*) *Infiltration*: Finally, the vacuum chamber is released to the atmospheric pressure. This is a key-step of the infiltration process: the pressure differential between the chamber and the holes forces the LC molecules to penetrate deeply into the pores. Temperature is a fundamental parameter since, during the infiltration procedure, the chamber is constantly kept at a temperature much higher than the clearing point (T = 110 °C). This has been proven to reduce the LC viscosity, thus favouring the pore infiltration, and to avoid wall contamination by humidity residuals. Heating the chamber before the PhC infiltration also allows the purification of the LCs, which is indeed extremely important. If LCs are not properly degassed, trapped gases may combine and generate bubbles inside the holes: heating and pumping the chamber makes the trapped gases boil out.

4. EXPERIMENTS AND DATA ANALYSIS

4.1 Trimming

The TE transmission spectra at room temperature through the ΓM-oriented PhC slabs (see Sect. 2) *before* (dark-grey lines) and *after* (black lines) infiltration with LC-K15 are shown in Fig. 6(a). Once the PhC is infiltrated with LCs, due to the reduced refractive index contrast $\Delta n = n_{eff} - n_{hole}$ between the semiconductor matrix and the holes, the photonic bandgap shrinks (*i.e.* $u = 0.215 - 0.28$) and the band edges red-shift. In particular, since for energies located in the air transmission band the electric field of the propagating Bloch modes is concentrated in the holes,[1] the energy shift $\Delta u_{Air} = - 5 \times 10^{-2}$ of the air band edge is one order of magnitude larger than the corresponding shift $\Delta u_{Diel} = - 5 \times 10^{-3}$ of the dielectric band edge. Moreover, after LC infiltration the transmission increases up to 70-80 % in the air band, thus indicating a strong reduction of out-of-plane-losses in the PhC slab. We remind that in low refractive index contrast planar PhCs perforating the vertical waveguide induces coupling of the guided wave to radiation modes into the claddings, thus resulting in out-of-plane losses.[28] When infiltrating PhCs with a material whose refractive index is higher than 1 (*i.e.* $n_{hole} > 1$), a weak vertical field confinement is introduced in the holes and out-of-plane losses are reduced.

The transmission spectra at room temperature through the FP cavity (see Sect. 2) *before* (dark-grey line; $a = 440$ nm) and *after* (black line; $a = 400$ nm) infiltration with LC-K15 are shown in Fig. 6(b). Like the two band edges, due to the increased n_{hole} value, also the FP resonance red-shifts with respect to the to the non-infiltrated case and is located at $u_{peak} = 0.2679$ (*i.e.* $\lambda_{peak} = a/u_{peak} = 1493$ nm) yielding an energy shift $\Delta u_{peak} = -1.38 \times 10^{-2}$, with $|\Delta u_{Diel}| << |\Delta u_{peak}| <$

$|\Delta u_{Air}|$. The FP peak was fitted using Eq. (1) with α_{WG} = 140 cm^{-1} [see Fig. 1(c)]. The calculated Airy's curve is shown in the inset of Fig. 6(b) (light grey dotted line) and the result of the fit is summarized in Table 1. Due to the reduced refractive index contrast Δn, after infiltration the PhC mirror transmission $T_{4\ rows}$ increases while its reflectivity $R_{4\ rows}$ decreases. Therefore, in agreement with the results obtained for simple PhC slabs, the loss coefficient $L_{4\ rows}$ decreases. Due to this change of the mirror optical properties and to the increased intracavity losses α_{WG}, the FP peak transmission increases (T_{peak} = 0.57 ± 0.01) and the cavity quality factor decreases (Q = 100 ± 5) with respect to the non-infiltrated cavity.

(a)   (b)
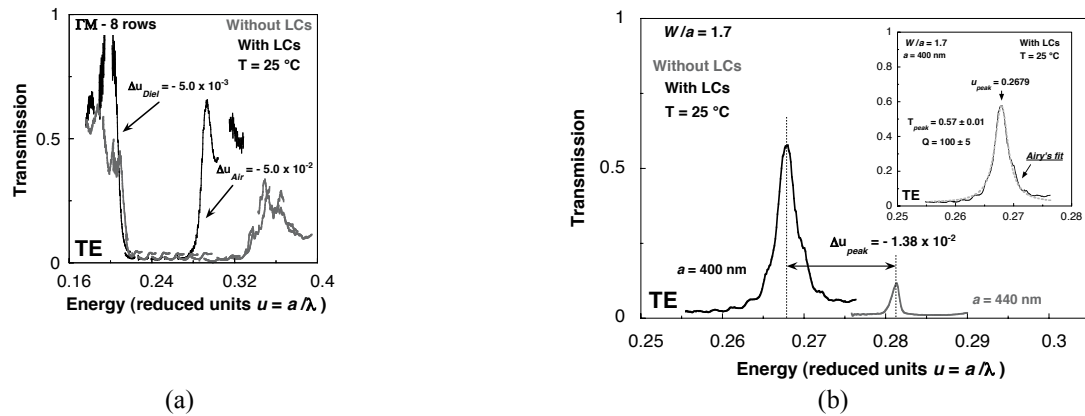
Figure 6: *Trimming (T = 25 °C)* - Experimental TE transmission spectra through (a) 8-rows thick ΓM-oriented PhC slabs and (b) a Fabry-Pérot (FP) cavity between two 4-rows thick ΓM-oriented PhC mirrors [see Figs. 2(b) and (c)] *before* (dark-grey lines) and *after* (black lines) LC infiltration. The values of the energy shift of the dielectric and air band edges (Δu_{Diel} and Δu_{Air}), and of the FP resonance (Δu_{peak}) are reported, respectively. The Airy's fit [see Eq. (1)] of the FP resonance is shown (dotted light-grey line) in the inset of (b): the FP resonance energy u_{peak}, the peak transmission T_{peak} and the cavity quality factor Q are indicated. The result of the Airy's fit is summarized in Table 1.

4.2   Optical characterization of the infiltration procedure

A systematic characterization of the infiltration procedure described in Sect. 3.3 was carried out by means of optical measurements. First of all, in order to assess the reproducibility and reliability of the technique several infiltration experiments were performed on the same sample under the same temperature, pressure and time conditions.

(a)   (b)
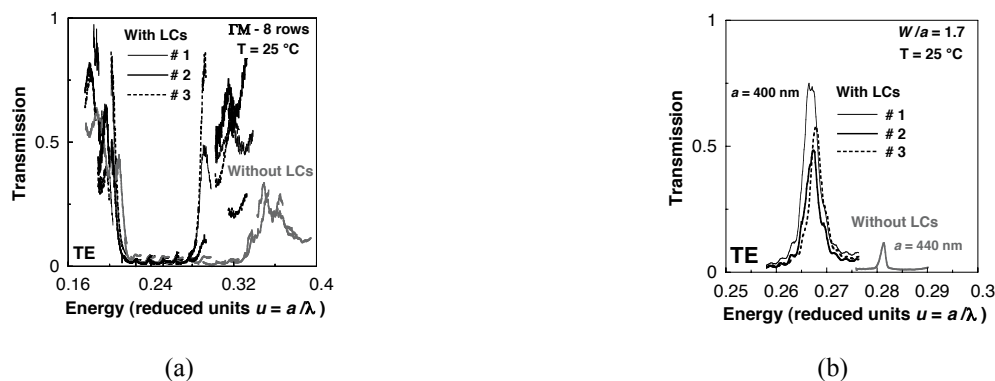
Figure 7: *Reproducibility (T = 25 °C)* - Experimental TE transmission spectra through (a) 8-rows thick ΓM-oriented PhC slabs and (b) a Fabry-Pérot (FP) cavity between two 4-rows thick ΓM-oriented PhC mirrors [see Figs. 2(b) and (c)] *after* three different infiltration procedures: # 1 (black solid lines), # 2 (thick black solid lines) and # 3 (thick black dotted lines). The spectra of the sample *before* infiltration (grey lines) are reported for comparison.

Before each infiltration the sample was heated at a temperature much higher than the clearing point T_{c1} (see Sect. 3.1) to evaporate the LC molecules, *i.e.* to empty completely the holes. In order to exclude the presence of LC residuals in the holes, after heating up to $T \gg T_{c1}$ the sample was cooled down to room temperature where the TE transmission spectra through the FP cavity were measured and compared with the reference spectrum *before* infiltration [see Fig. 3(b)].

The TE transmission spectra at room temperature through the simple PhC slabs and the FP cavity (see Sect. 2) *after* three different infiltration procedures (# 1: black solid lines, # 2: thick black solid lines, and # 3: thick black dotted lines) are shown in Figs. 7 (a) and (b), respectively. While the fluctuations of the transmission values in the dielectric (air) bands as well as of the FP peak transmission may be due to measurement uncertainties and/or to sample degradation (*e.g.* damaging of the cleaved facet),[24] both the band edges and the FP resonance are always located at the same energy after all the infiltrations. This proves the great reproducibility and reliability of our in-filling technique in terms of infiltration efficiency (see below).

As it is shown in Ref. (13), the filling degree of the infiltrated PhCs is a critical parameter, whose measurement is not trivial. For instance, due to the particular morphology and geometry of planar PhCs, the use of standard scanning electron or atomic force microscopy is not straightforward. Moreover, these techniques have an intrinsic limit when applied to such systems:[24,28] they can only provide local information on a very limited number of holes. On the other hand optical measurements have already been proved to be very useful in the characterization of planar PhCs: for example the average f value can be easily obtained by fitting ILS transmission spectra.[24,28] Here the average infiltration efficiency η was accurately determined by measuring the TE and TM transmission spectra [black lines in Figs. 8(a) and (b), respectively] through *infiltrated* PhC slabs (see Sect. 2) at a temperature $T = 40\ °C > T_{c1}$. Due to the birefringence of nematic LCs, their refractive index n_{LC} is a tensor and its value indeed depends on the molecule orientation with respect to the electric field. However, when working at a temperature higher than the clearing point, LCs are in the isotropic phase and n_{LC} is just a scalar quantity independent from the molecule orientation, *i.e.* $n_{LC} = n_i$.

(a)   (b)
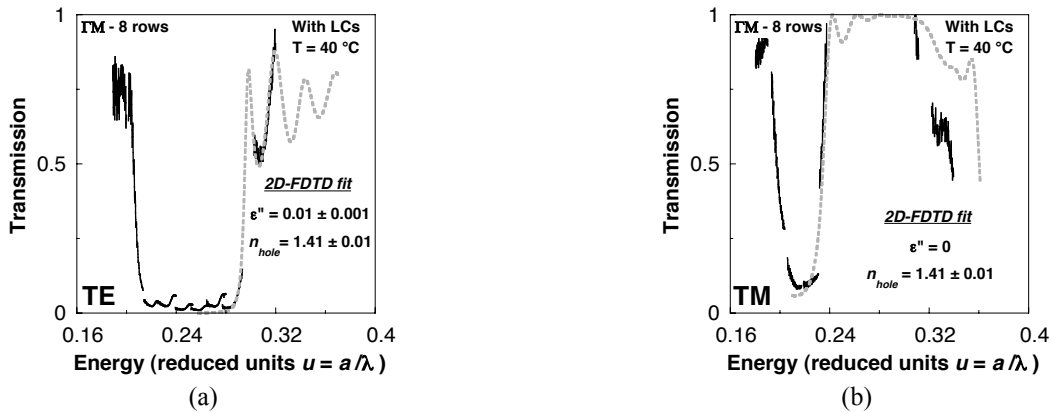
Figure 8: *With liquid crystals (T = 40 °C)* - Experimental (black lines) and calculated (light grey dotted lines) (a) TE and (b) TM transmission spectra through *infiltrated* 8-rows thick ΓM-oriented PhC slabs [see Fig. 2(b)]. The values of the loss parameter $ε''$ and the hole refractive index n_{hole} obtained from the 2D-FDTD fit of the air transmission bands are reported, respectively.

While a well-defined stopgap with steep band edges appears in the frequency range $u = 0.216 - 0.29$ for the TE spectrum, only a small pseudo-gap opens up in the TM transmission ($u \approx 0.21 - 0.23$).[1] We remark that, due to the temperature increase, both band edges blue-shift in the TE transmission with respect to the room temperature spectra [see Fig. 6(a)]: $\Delta u_{Diel-T} = + 1 \times 10^{-3}$ and $\Delta u_{Air-T} = + 1 \times 10^{-2}$, with as usual[1] $|\Delta u_{Air-T}| \gg |\Delta u_{Diel-T}|$ (see Sect. 4.4 for details). Moreover, as for the TE transmission, values as high as 80-90% are reached in the air band, thus indicating a further reduction of out-of-plane losses with respect to the room temperature case. The air band transmission spectra were fitted by means of the same 2D-FDTD model as the one described in Sect. 2 with $ε''$ and n_{hole} as free fitting parameters. In order to take into account the temperature dependence of the semiconductor refractive indexes,[25] the values $n_{eff} = 3.243$ and 3.233 were assumed for the TE and TM waveguide effective refractive indexes, respectively [see Fig. 1(b)]. Finally, the value $f = 0.42$ was taken for the air filling factor [see Fig. 3(a)]. The calculated spectra are shown in Fig. 8 (light grey dotted lines). Concerning losses, while the value $ε'' = 0.010 \pm 0.001$ was obtained for the TE polarization, $ε'' = 0$

was taken for the TM polarization, since in this case only the fit of the energy position of the pseudo-air band edge (depending on the n_{hole} value) is meaningful. The fit yielded the same value $n_{hole} = 1.41 \pm 0.01$ for both polarizations, thus confirming that at T = 40 °C the infiltrated LCs are in their isotropic phase. The same result is obtained by the 2D-FDTD (or 2D-PWE) fit of the resonance located at $u_{peak} = 0.2667$ in the transmission spectrum through the FP cavity at T = 40 °C [see Fig. 9(a)]. Since the infiltration efficiency can be written as

$$\eta = \frac{n_{hole} - 1}{n_{LC} - 1} \tag{2}$$

and $n_{LC} = n_i = 1.575$ for $\lambda = 1.5$ µm at T = 40 °C [see Fig. 4(b)],[31] the value $\eta = 0.71 \pm 0.02$ is obtained. We remark that the latter is an average value for the infiltrated PhC slab: it doesn't contain any information on the partial or complete filling of single pores.

4.3 Temperature tuning

The temperature tuning of the planar PhC structures after infiltration with LC-K15 was investigated in details by measuring the transmission through the FP cavity (see Sect. 2) at different temperatures. First of all, as in Ref. (13), in order to exploit the large refractive index change due to the nematic-to-isotropic LC phase transition, the temperature of the sample was increased to a value well above the clearing point, *i.e.* T = 40 °C. Then the temperature was decreased down to T = 10 °C with steps $\Delta T = 2$ °C.

The transmission spectra *before* (dark-grey line; a = 440 nm) and *after* (a = 400 nm) infiltration for T = 25 °C (dotted black line) and T = 40 °C (solid black line) are shown in Fig. 9(a). As in Sect. 4.1 the FP peak was fitted using Eq. (1) with $\alpha_{WG} = 140$ cm^{-1} [see Fig. 1(c)]. The calculated Airy's curve is shown in the inset of Fig. 9(a) (light grey dotted line) and the result of the fit is summarized in Table 1.
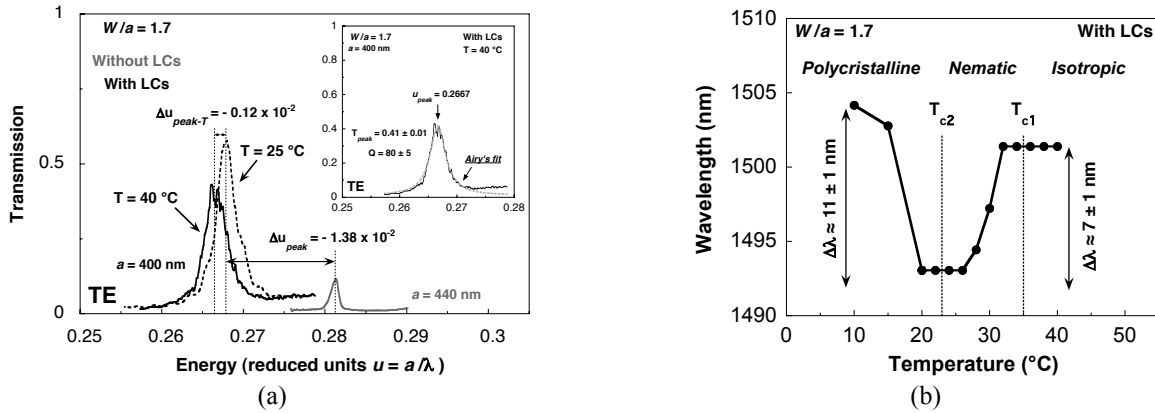
Figure 9: *Tuning* - (a) Experimental TE transmission spectra through a Fabry-Pérot (FP) cavity between two 4-rows thick ΓM-oriented PhC mirrors [see Figs. 2(b) and (c)] *before* (dark grey line) and *after* liquid crystal infiltration for T = 25 °C (dotted black line) and T = 40 °C (solid black line). The values of the energy shift of the FP resonance due to the LC infiltration (Δu_{peak}) and to the temperature tuning (Δu_{peak-T}) are reported. The Airy's fit [see Eq. (1)] of the FP resonance is shown in the inset (dotted light-grey line): the FP resonance energy u_{peak}, the peak transmission T_{peak} and the cavity quality factor Q are indicated. The result of the Airy's fit is summarized in Table 1; (b) FP resonance wavelength as a function of temperature after LC infiltration. The wavelength shift values $\Delta\lambda$ obtained at T = 10 °C and T = 40 °C are reported. The nematic-to-isotropic and nematic-to-polycrystalline phase transition temperatures [T_{c1} (clearing point) and T_{c2} (melting point), respectively] for the bulk LC material are indicated for comparison.

The PhC mirror reflectivity $R_{4\ rows}$ decreases and the transmission $T_{4\ rows}$ is constant, so that both the FP peak transmission ($T_{peak} = 0.41 \pm 0.01$) and the cavity quality factor (Q = 80 ± 5) decrease with respect to T = 25 °C. On the other hand, the loss coefficient $L_{4\ rows}$ increases when increasing the temperature, which is apparently in contrast with what is observed for simple PhC slabs where the loss parameter ε'' decreases when increasing the temperature (Sect. 4.2). As for the resonance tuning, differently from the band edges (see Sect. 4.2) but in agreement with Ref. (13), after infiltration the FP peak red-shifts with increasing temperature (see Sect. 4.4 for details) and is located at $u_{peak} = 0.2667$

(*i.e.* $\lambda_{peak} = a/u_{peak} = 1500$ nm). The energy shift $\Delta u_{peak\text{-}T} = -0.12 \times 10^{-2}$ is one order of magnitude smaller than the shift $\Delta u_{peak} = -1.38 \times 10^{-2}$ obtained at room temperature with respect to the non-infiltrated case (*trimming*, see Sect. 4.1). Nevertheless, the effect is stronger than the results obtained in Ref. (25), where the thermal dependence of the semiconductor refractive indexes was exploited to finely tune the optical response of InP-based FP cavities. In both cases the FP resonance red-shifts with temperature, but, while in Ref. (25) the gradient value $\Delta\lambda/\Delta T \approx 0.1$ nm/°C was obtained, *i.e.* a wavelength shift $\Delta\lambda = 2$ nm for $T = 20\text{-}40°C$, here the combination of the semiconductor and the LC refractive index thermal dependence yields an overall shift $\Delta\lambda = 7 \pm 1$ nm [see Fig. 9(b)]. Therefore, the LC infiltration allows a larger temperature tuning of the optical properties of PhC devices.

The wavelength location of the FP resonance as a function of temperature is shown in Fig. 9(b). In the temperature range around 20 °C the peak wavelength is nearly constant since neither the semiconductor nor the LC refractive indexes change significantly. On the other hand, the resonance wavelength sharply increases above 28 °C and below 20 °C with $\Delta\lambda = 7 \pm 1$ nm and $\Delta\lambda = 11 \pm 1$ nm, respectively. As it is shown in Sect. 4.1, the increase of the resonance wavelength (*i.e.* the energy red-shift) is due to the increase of n_{hole} (*i.e.* of n_{LC}), which, in the first case, comes from the nematic-to-isotropic LC phase transition, whilst in the second case is linked to the nematic-to-polycrystalline LC phase transition.[32-33] We note that, due to the confinement effects induced by the hole sidewalls on the LC molecules,[32-33] the temperature of the LC phase transitions inside the holes are slightly lower than their bulk values T_{c1} and T_{c2} (see Sect. 3.1). It was thus demonstrated that after LC infiltration a symmetrical tuning of the FP resonance can be obtained by either increasing or decreasing the temperature.

(a)   (b)
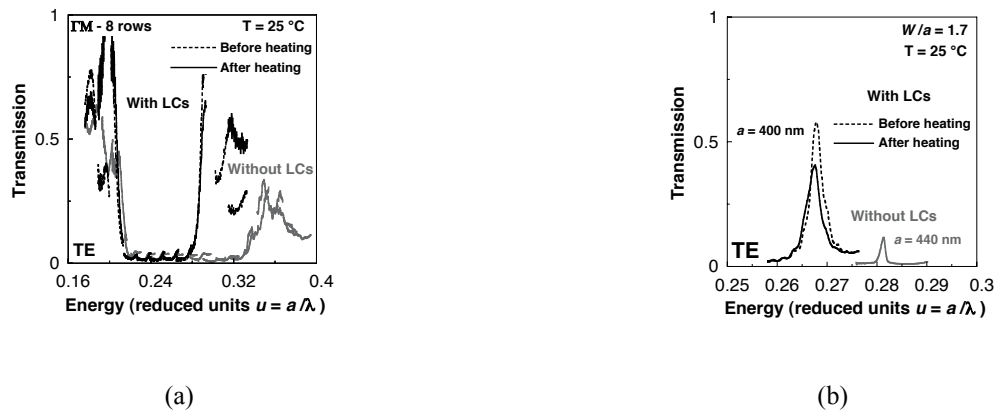
Figure 10: *Reversibility (T = 25 °C)* - Experimental TE transmission spectra through (a) 8-rows thick ΓM-oriented PhC slabs and (b) a Fabry-Pérot (FP) cavity between two 4-rows thick ΓM-oriented PhC mirrors [see Figs. 2(b) and (c)] *before* (black dotted lines) and *after* (black solid lines) heating the sample up to 40 °C. The spectra of the sample *before* infiltration (grey lines) are reported for comparison.

Finally, the reversibility of the temperature tuning of the infiltrated FP cavity was checked. After heating up to $T = 40$ °C the sample was cooled down to room temperature where the TE transmissions through the PhC slabs and the FP cavity (see Sect. 2) were measured. As it is illustrated in Fig. 10, the spectra *before* (black dotted lines) and *after* (black solid lines) heating the sample were compared: While, as in Sect. 4.2, the fluctuations of the transmission values in the dielectric (air) bands as well as of the FP peak transmission may be due to measurement uncertainties and/or to sample degradation (*e.g.* damaging of the cleaved facet),[24] both the band edges and the FP resonance are located at the same energy before and after heating. This proves that the complete heating-cooling cycle affects neither the infiltration efficiency (*i.e.* the LC molecules don't evaporate at $T = 40$ °C) nor the LC orientation (*i.e.* hysteresis effects are negligible), so that the temperature tuning is fully reversible.

4.4 Molecule orientation

When infiltrating nematic liquid crystals in porous materials made of cylindrical cavities, like planar PhCs, the equilibrium configuration of the molecules inside the pores depends primarily on the anchoring of the LC director to the lateral surface of the pores and then on confinement effects linked to the LC properties (*e.g.* the LC elastic moduli), to the cavity itself (*e.g.* its size), and to the sidewall surface (*e.g.* its chemical state, the presence of roughness).[32-33] Here

we show how the optical measurements described in the previous sections can be used to deduce the average molecule orientation in infiltrated planar PhCs.

All the possible configurations of nematic LCs in a cylindrical cavity can be grouped into two main families according to the prevalent orientation of their directors:[32-33] (*i*) *parallel*: most of the LC molecules are parallel to the hole axis; and (*ii*) *perpendicular*: most of the LC molecules are aligned on planes perpendicular to hole axis. In the first case (*parallel*) the LC molecules would be perpendicular and parallel to the electric field (*i.e. $n_{LC} = n_o$ and $n_{LC} = n_e$*) for the TE and TM polarization, respectively. In the second case (*perpendicular*), while in the TM polarization the LC molecules would be perpendicular to the electric field (*i.e. $n_{LC} = n_o$*), for the TE polarization n_{LC} would be a tensor, its value depending on the exact director configuration and on the electric field map. The corresponding values of the LC refractive index n_{LC} inside the holes, as well as the values of the hole refractive index n_{hole} calculated for $\eta = 0.71$ with Eq. (2) are reported in Table 2.

LC configuration	Polarization	n_{LC}	n_{hole} ($\eta = 0.71$)
Parallel	TE	$n_o = 1.516$	1.366
	TM	$n_e = 1.682$	1.484
Perpendicular	TE	tensor	-
	TM	$n_o = 1.516$	1.366

Table 2: Liquid crystal (LC) refractive index values n_{LC} inside the PhC holes for the two possible molecule configurations *parallel* and *perpendicular* to the hole axis and for both polarization directions (TE and TM). The ordinary n_o and extraordinary n_e refractive index values of LC-K15 are derived from Ref. (31) [see also Fig. 4(b)]. The corresponding hole refractive index values n_{hole} calculated from Eq. (2) for an infiltration efficiency $\eta = 0.71$ are also reported.

The TE transmission spectrum through the *infiltrated* ΓM-oriented PhC slabs shown in Fig. 6(a) is reported in Fig. 11(a) and compared with the corresponding TM spectrum [see Fig. 11(b)] (black lines).

(a)   (b)
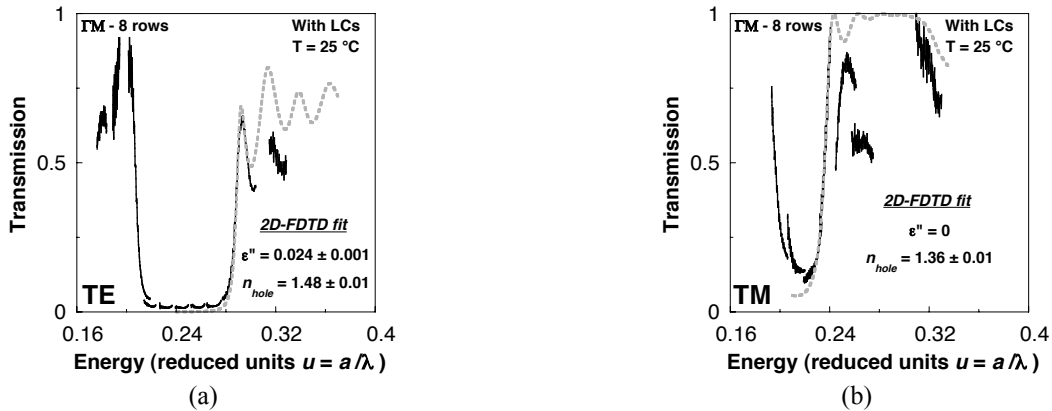
Figure 11: *With liquid crystals (T = 25 °C)* - Experimental (black lines) and calculated (light grey dotted lines) (a) TE and (b) TM transmission spectra through *infiltrated* 8-rows thick ΓM-oriented PhC slabs [see Fig. 2(b)]. The values of the loss parameter ε'' and the hole refractive index n_{hole} obtained from the 2D-FDTD fit of the air transmission bands are reported, respectively.

The air band transmission spectra were fitted by means of the same 2D-FDTD model as the one described in Sect. 2 with ε'' and n_{hole} as free fitting parameters. The values $n_{eff} = 3.24$ and 3.23 were assumed for the TE and TM waveguide effective refractive index, respectively [see Fig. 1(b)].[25] Finally, the value $f = 0.42$ was taken for the air filling factor [see Fig. 3(a)]. The calculated spectra are shown in Fig. 11 (light grey dotted lines). Concerning losses, the value $\varepsilon'' = 0.024 \pm 0.001$ was obtained for the TE polarization, thus confirming the reduction of out-of-plane losses when increasing the temperature in PhC slabs [see Sect. 4.2 and Fig. 8(a)]. On the other hand, as in Sect. 4.2, $\varepsilon'' = 0$ was taken for the TM polarization. The fit yielded the values $n_{hole} = 1.48 \pm 0.01$ and $n_{hole} = 1.36 \pm 0.01$ for TE and TM, respectively. Comparing these results with Table 2, we can deduce that the LC molecules are aligned on planes *perpendicular* to the hole axis. This is further supported by the temperature dependence of n_{hole} for the TM polarization:

since n_{hole} slightly increases with temperature [*i.e.* the air bad edge slightly red-shifts: see Figs. 8(b) and 11(b)], we can conclude that $n_{hole} \propto n_o$. Our conclusion on the molecule orientation is in contrast Ref. (13), where, on the other hand, only TE transmission measurements were considered.

For the TE polarization, using Eq. (2) we can calculate the LC refractive index $< n_{LC} >_{slab} = 1.675 \pm 0.015$, which is an average of n_o and n_e weighted on the local electric field map. $< n_{LC} >_{slab}$ is higher than the isotropic refractive index n_i, thus explaining why in the transmission spectra through infiltrated PhC slabs when increasing the temperature the band edges blue-shift. We note that the 2D-FDTD (or 2D-PWE) fit of the FP resonance of the infiltrated cavity [see Fig. 6(b)] yields $n_{hole} = 1.39 \pm 0.01$, *i.e.* the average value $< n_{LC} >_{FP} = 1.550 \pm 0.015$. Differently from the PhC slabs, the latter value is slightly lower than n_i so that after infiltration the FP resonance red-shifts with temperatures (see Sect. 4.3). This discrepancy between $< n_{LC} >_{slab}$ and $< n_{LC} >_{FP}$ as well the different behavior of the loss parameters with respect to temperature variations in the infiltrated PhC slabs and cavities may be due (*i*) to the different electric field map in the transmission band (slabs) and in the photonic bandgap (cavity), and (*ii*) to the fact that the real LC molecule configuration is 3D, while the theoretical models used here are all 2D. A phenomenological analysis of the local electric field map will be published elsewhere, while 3D calculations (*e.g.* 3D-FDTD) are necessary to model exactly the effects of the LC molecule orientation on the optical properties of the infiltrated PhC structures.

5. CONCLUSIONS

In conclusion, the trimming and temperature tuning of the optical properties of planar PhCs by LC infiltration have been demonstrated. With respect to the preliminary studies of Ref. (13) (*i*) a reproducible and reliable infiltration procedure has been developed and characterized, which allows the control of all the infiltration parameters (*e.g.* temperature and pressure) and, when necessary, the modification of the surface chemical state;[23] (*ii*) the infiltration efficiency was accurately determined by means of optical measurements; and (*iii*) the molecule orientation inside the holes was carefully deduced showing that transmission measurements as a function of both temperature and polarization are necessary to study the LC director configuration in the confined system. In particular the LC molecules were found to be aligned on planes perpendicular to the hole axis. Such a configuration opens the way to the electrical and optical tuning of PhC devices. This is even more important when considering that, as it was observed in Ref. [APL-BW], while the temperature tuning of a PhC structure can be extremely practical at the laboratory level, due to its intrinsically slow repetition rate and to the large thermal conductivity of III-V semiconductors, it will be very difficult to exploit it in real integrated optics devices. However, it is worth noting that trimming and temperature tuning by liquid crystal infiltration can be still used to compensate for fabrication imperfections, out-of-plane losses, etc.

ACKNOWLEDGEMENTS

REFERENCES

1. *Photonic Crystals*, edited by K. Busch, S. Lölkes, R.B. Wehrspohn, and H. Föll, Wiley-VCH, Weinheim, 2004.
2. K. Yoshino, Y. Kawagishi, M. Ozaki, and A. Kose, "Mechanical tuning of the optical properties of plastic opal as a photonic crystal", *Japanese Journal of Applied Physics Part 2* **38**, pp. L786-L788, 199.
3. A. Figotin, Y.A. Godin, and I. Vitebsky, "Two-dimensional tunable photonic crystals", *Physical Review B* **57**, pp. 2841-2848, 1998.
4. C. Kee, J. Kim, H.Y. Park, I. Park,, "Two-dimensional tunable magnetic photonic crystals", *Physical Review B* **61**, pp. 15523-15525, 2000.

5. G. Mertens, T. Röder, H. Matthias, H. Marsmann, H.-S. Kitzerow, S.L. Schweizer, C. Jamois, R.B. Wehrspohn, and M. Neubert, "Two- and three-dimensional photonic crystals made of macroporous silicon and liquid crystals", *Applied Physics Letters* **83**, pp. 3036-3038, 2003.

6. E.P. Kosmidou, E.E. Kriezis, and T.D. Tsiboukis, "Analysis of tunable photonic crystal devices comprising liquid crystal materials as defects", *IEEE Journal of Quantum Electronics* **41**, p. 657-665, 2005.

7. K. Busch, and S. John, "Liquid-crystal photonic-band gap materials. The tunable electromagnetic vacuum", *Physical Review Letters* **83**, pp. 967-970, 1999.

8. S. Gottardo, D. S. Wiersma, and W.L. Vos, "Liquid crystal infiltration of complex dielectrics", *Physica B* **338**, pp. 143-148 2003.

9. R. Ozaki, M. Ozaki, and K. Yoshino, "Light propagation analysis and high-speed electr-optic switching in one-dimensional photonic crystal with nematic liquid crystal defect layer", *Electronics and Communications in Japan Part 2* **88**, pp. 46-53, 2005.

10. S.M. Weiss, H. Ouyang, J. Zhang, and P.M. Fauchet, "Electrical and thermal modulation of silicon photonic bandgap microcavities containing liquid crystals", *Optics Express* 13, pp. 1090-1097, 2005.

11. S.M. Weiss, M. Haurylau, and P.M. Fauchet, "Tunable photonic bandgap structures for optical interconnects", *Optical Materials* **27**, pp. 740-744, 2005.

12. S.M. Weiss, and P.M. Fauchet, "Electrically tunable porous silicon active mirrors", *Physica Status Solidi (a)* **197**, pp. 556-560, 2003.

13. Ch. Schuller, F. Klopf, J.P. Reithmaier, M. Kamp, and A. Forchel, "Tunable photonic crystals fabricated in III-V semi-conductor slab waveguides using infiltrated liquid crystals", *Applied Physics Letters* **82**, pp. 2767-2769, 2003.

14. S.W. Leonard, J.P. Mondia, H. M. van Driel, O. Toader, S. John, K. Busch, A. Birner, U. Gösele, and V. Lehmann, "Tunable two-dimensional photonic crystals using liquid-crystal infiltration", *Physical Review B* **61**, pp. R2389-R2392, 2000.

15. G. Mertens, T. Röder, R. Schweins, K. Huber, and H.-S. Kitzerow, "Shift of the photonic band gap in two photonic crystal/liquid crystal composites", *Applied Physics Letters* **80**, pp. 1885-1887, 2002.

16. K. Yoshino, Y. Shimoda, Y. Kawagishi, K. Nakayama, and M. Ozaki, "Temperature tuning of the stop band in transmission spectra of liquid-crystal infiltrated synthetic opal as tunable photonic crystal", *Applied Physics Letters* **75**, pp. 932-934, 1999.

17. S. Kubo, Z.-Z. Gu, K. Takahashi, Y. Ohko, O. Sato, and A. Fujishima, "Control of the optical band structure of liquid crystal infiltrated inverse opal by a photoinduced nematic-isotropic phase transition", *Journal of the American Chemical Society* **124**, pp. 10950-10951, 2002.

18. S. Kubo, Z.-Z. Gu, K. Takahashi, A. Fujishima, H. Segawa, and O. Sato, "Tunable photonic band gap crystals based on a liquid crystal-infiltrated inverse opal structure", *Journal of the American Chemical Society* **126**, pp. 8314-8319, 2004.

19. Y. Shimoda, M. Ozaki, and K. Yoshino, "Electric field tuning of a stop band in a reflection spectrum of synthetic opal infiltrated with nematic liquid crystal", *Applied Physics Letters* **79**, pp. 3627-3629, 2001.

20. D. Kang, J. E. Maclennan, N.A. Clark, A. A. Zakhidov, and R.H. Baughman, "Electro-optic behaviour of liquid-crystal-filled silica opal photonic crystals: effect of liquid-crystal alignment", *Physical Review Letters* **86**, pp. 4052-4055, 2001.

21. F. Du, Y.-Q. Lu, and S.-T. Wu, " Electrically tunable liquid-crystal photonic crystal fiber", *Applied Physics Letters* **85**, pp. 2181-2183, 2004.

22. A. Urbas, V. Tongiglia, L. Natarajan, R. Sutherland, H. Yu, J.-H. Li, and T. Bunning, "Optically switchable liquid crystal photonic structures", *Journal of the American Chemical Society* **126**, pp. 13580-13581, 2004.

23. Martz, L. Zuppiroli, and F. Nüesch, "Benzoic and aliphatic carboxylic acid monomolecular layers on oxidized GaAs surfaces as a tool for two-dimensional photonic crystal infiltration", *Langmuir* **20**, pp. 11428-11432, 2004.

24. R. Ferrini, D. Leuenberger, M. Mulot, M. Qiu, J. Moosbürger, M. Kamp, A. Forchel, S. Anand, and R. Houdré, "Optical study of two-dimensional InP.based photonic crystals by internal light source technique", *IEEE Journal of Quantum Electronics* **38**, p. 786-799, 2002.

25. B. Wild, R. Ferrini, R. Houdré, M. Mulot, S. Anand, and C.J.M. Smith, "Temperature tuning of the optical properties of planar photonic crystal microcavities", *Applied Physics Letters* **84**, pp. 846-848, 2004.

26. M. Mulot, R. Ferrini, B. Wild, J. Moosburger, A. Forchel, R. Houdré, and S. Anand, "Fabrication of 2D InP-based photonic crystals by chlorine based chemically assisted ion beam etching", *Journal of Vacuum Science and Technology B* **22**, pp. 707-709, 2004.

27. M. Qiu, B. Jaskorzynska, M. Swillo, and H. Benisty, "Time-domain 2D modeling of slab-waveguide based photonic-crystal devices in the presence of out-of-plane radiation losses", *Microwave and Optical Technology Letters* **34**, pp. 387-393, 2002.

28. R. Ferrini, R. Houdré, H. Benisty, M. Qiu, and J. Moosburger, "Radiation losses in planar photonic crystals: two-dimensional representation of hole depth and shape by an imaginary dielectric constant", *Journal of the Optical Society of America B* **20**, pp. 469-478, 2003.

29. M. Plihal, and A.A. Maradudin, "Photonic band-structure of 2-dimensional systems – the triangular lattice", *Physical Review B* **44**, pp. 8565-8571, 1991.

30. JT. Mansare, R. Decressain, C. Gors, and V.K. Dolganov, "Phase transformations and dynamics of 4-cyano-4'-pentylbiphenyl (5CB) by nuclear magnetic resonance, analysis differential scanning calorimetry, and wide-angle X-ray diffraction analysis", *Molecular Crystals and Liquid Crystals Science and Technology A: Molecular Crystals and Liquid Crystals* **382**, pp. 97-111, 2002.

31. Jun Li, and Shin-Tson Wu, "Extended Cauchy equations for the refractive indexes of liquid crystals", *Journal of Applied Physics* **95**, pp. 896-901, 2004.

32. G. P. Crawford, and S. Zumer, *Liquid Crystals in Complex Geometries: Formed by Polymer and Porous Networks*, Taylor & Francis, London, 1996.

33. S.V. Burylov, "Equilibrium configuration of a nematic liquid crystal confined to a cylindrical cavity", *Journal of experimental and theoretical physics* **85**, pp. 873-886, 1997.